

Research

Online tracking of dynamically time-varying inertia using an enhanced SDFT-based estimation methodology

David Ceulemans^{1,2} · Foeke Vanbecelaere^{3,4} · Nick Van Oosterwyck^{1,2} · Jasper De Viaene^{3,4} · Jan Steckel^{2,5} · Stijn Derammelaere^{1,2}

Received: 31 August 2023 / Accepted: 28 February 2024

Published online: 09 April 2024

© The Author(s) 2024 [OPEN](#)

Abstract

The overall motion performance of mechatronic machines depends heavily on proper knowledge of the machine's characteristics, among which the inertia. Moreover, the inertia of most multi-body mechanisms, for example, reciprocating slider-crank mechanisms, varies as a function of the machine position, thereby challenging optimal control. Nevertheless, the inertia's variation is sometimes not known accurately enough or changes over time due to, e.g. a production process or premature wear, forcing an online control/correction of the inertia profile. Therefore, earlier, the author developed a new computational-friendly online method based on a frequency-specific magnitude response to estimate the machine's position-dependent load side inertia, assuming good knowledge of all other machine properties. Yet, to guarantee accuracy, the maximum machine speed during estimation had to be strongly reduced, resulting in an undesirable longer motion time. Therefore, in this work, the failure mechanism of the earlier proposed estimator is analysed and overcome by intelligently separating estimation and motion signals. As a result, the estimator is no longer limited by the machine's motion speed but rather by a maximum in the inertia variation per signal excitation period and, thus, time. Moreover, given this limiting variation, a guideline was established to evaluate the new method's estimation quality. Finally, both in simulation and on a physical machine, by taking advantage of the newly proposed method, the minimal required estimation time is reduced significantly (up to 50% on the machine) without diminishing the estimation accuracy.

Keywords Online inertia estimation · Online parameter estimation · System identification · SDFT

Foeke Vanbecelaere, Nick Van Oosterwyck, Jasper De Viaene, Jan Steckel and Stijn Derammelaere have contributed equally to this work.

✉ David Ceulemans, david.ceulemans@uantwerpen.be; Foeke Vanbecelaere, foeke.vanbecelaere@ugent.be; Nick Van Oosterwyck, nick.vanoosterwyck@uantwerpen.be; Jasper De Viaene, jasper.deviane@ugent.be; Jan Steckel, jan.steckel@uantwerp.be; Stijn Derammelaere, stijn.derammelaere@uantwerp.be | ¹Departement of Electromechanics, CoSysLab, University of Antwerp, Groenenborgerlaan 171, 2020 Antwerp, Belgium. ²AnSyMo/CoSys, Flanders Make, the strategic research center for the manufacturing industry, Antwerp, Belgium. ³Department of Electrical Energy, Metals, Mechanical Constructions and Systems, University of Ghent campus Kortrijk, Kortrijk, Belgium. ⁴EEDT-MP, Flanders Make, the strategic research center for the manufacturing industry, Antwerp, Belgium. ⁵Departement of Electronics, CoSysLab, University of Antwerp, Groenenborgerlaan 171, 2020 Antwerp, Belgium.



1 Introduction

1.1 Motivation

Repetitive reciprocating movements with machine-standstill at both extremes, frequently referred to as rest-to-rest (RtR) motions, characterize numerous high-dynamic industrial applications. To drive these movements, machine builders often use a single-axis-driven multi-body mechanism, e.g., a slider-crank mechanism, because of the inherent conversion from rotation to a more complex motion and its control simplicity [3]. Furthermore, during the machine design phase, machine builders typically only define the RtR start and end positions, allowing the optimization of the intermediate position profile to, e.g., minimal motion time [2], minimal energy usage [22], or minimal peak motor torque [21]. Nevertheless, since the optimization is usually model-based, the eventual yield of the optimized trajectory depends heavily on the accurate knowledge of the system properties such as inertia, load torque, and friction. Given the multi-body mechanism, the machine load properties often vary as a function of the motor's position. Consequently, accurate knowledge of inertia's time/position dependence is indispensable to exploit the potential of trajectory optimization fully.

1.2 Related work

Previous work showed that the inertia of the load system could be calculated analytically [24] or extracted with high accuracy using CAD motion simulations assuming an accurate 3D model [21]. However, in various scenarios, as illustrated in Fig. 1, the mass and, thus, the inertia at the load side changes regularly, e.g., because of varying machine loads. Consequently, a method that doesn't necessitate a standstill, referred to as an online method, is required to ensure continuous optimal performance.

Specific literature on the online estimation of position-dependent system properties of a 2-mass model, shown in Fig. 2, is relatively scarce. Nevertheless, much research has been done in the past decades on estimating one or more time-variant system properties. The state-of-the-art can be divided into direct estimation methods based on, e.g., the least squares [1, 5, 16] or Kalman filters [18, 19], and indirect methods [4, 6, 10, 11, 13] approximating the unknown variables through a (non-)linear combination of standard functions such as polynomials or wavelets.

Direct estimation based on the least-squares has been widely described and argued in the literature. [16] demonstrated that LS could fit the position and hence time-dependent variables of a linearised two-mass model. Although [16] proves the effectiveness, it is well known that LS-based algorithms are sensitive to initial conditions and noise and can converge slowly, which makes them less suitable for online identification of relatively fast varying parameters

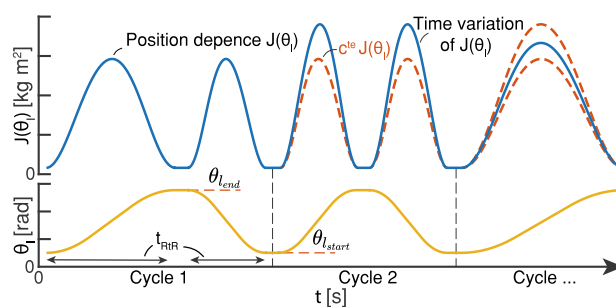


Fig. 1 Illustration of the inertia J as a function of machine position θ_i , and the time variation of the position dependant inertia $J(\theta_i)$

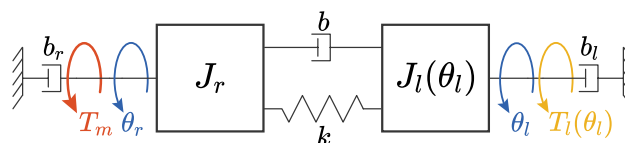


Fig. 2 A basic two-mass model with position-dependent inertia $J_l(\theta_l)$ and load torque $T_l(\theta_l)$

[10, 13, 14]. Also, Kalman filters, known for their excellent estimation performance under noisy conditions, can be used to estimate a system's frequency response [15]. Both [19] and [18] estimated the time-varying inertia using an (extended) Kalman filter, respectively, in simulation and on a physical slider-crank mechanism. Yet, given the relatively slow variation of the system properties over time (respectively ± 0.025 and ± 0.02 kg·m²/s), the accuracy of both estimation results is unsatisfying. Moreover, as noted in [18], proper knowledge of the initial state and noise properties is vital for fast and accurate convergence. Also, an advanced estimator, such as the Sigma-Point Kalman filter [20], is promising for inertia estimation but converges relatively slowly, as shown in [17]. Fixed-time observers, guaranteed to converge within a pre-specified time interval, have already demonstrated excellent results in the literature but require the design of gain factors [9], which is less straightforward for machine builders.

The principle of the indirect estimators is based on basic function expansion within a considered (time) frame. Generally, the idea is to approximate/expand the time-varying parameters by a (non-)linear combination of a predefined set of basic functions so that the estimation problem is rephrased to the regression selection of functions and the estimation of these function's constant coefficients [10]. Recently, progress has been made in this area, resulting in a wide range of proven basis functions (e.g., polynomials, wavelets, B-splines, etc.) with each of their advantages. In [4], the time-dependent stiffness of a mass-spring-damper system is estimated with LS by approximating it as linear varying within the considered window. [13] approximated the time-varying properties of a generic servomechanism through polynomials using a Taylor expansion. Employing multi-wavelet decomposition, [6] showed that a single mass-spring-damper system's discrete varying stiffness could be more adequately tracked than a classical RLS algorithm with a forgetting factor. Nevertheless, as referred to in [10], an unknown inertia variation requires a solid basis of standard functions to approximate its instantaneous value. Therefore, an indirect method may require much computational effort. Hence, given the often real-time character of the estimation, the computational requirements may undermine the implementation on an, e.g., an industrial motor drive, making this second group of indirect methods less applicable.

1.3 Contribution

In [24] and [25], the authors of this paper developed a new method to estimate the time-dependent inertia of a two-mass system. Similar to [16], the time-varying property is tracked through a frequency-specific gain employing a discrete Fourier transform (DFT) filter, followed by a mathematical conversion to the inertia via the system's transfer function. Contrary to the indirect methods, this principle only requires analyses of a single frequency, limiting the required real-time computational power. Moreover, unlike most direct estimation methods, thanks to the spectral filter, the new method convergence time is fixed to the fundamental period of the excitation signal. Besides, it has the inherent property of eliminating noise, making it an attractive technique. However, as explained in [25], the use of [24] imposes requirements on the minimum disturbance-to-position (DRP) ratio, eventually limiting the minimal motion time. As a result, [25] prolongs the minimum feasible motion time by a factor of 10 to the original motion time. Thus, the current DRP ratio restricts using [24] at higher machine speeds. Nevertheless, convinced of [24]'s added value, this work's main objective is to decrease the minimum achievable motion time. To this end, this work analyses the failure mechanism(s) at high speed/lower motion time and, as the main contribution, formulates the following improvement to the existing methodology to enable high-speed estimation:

As deduced in this paper, the [25] estimator's failure at lower rest-to-rest motion times is mainly due to the insufficiently accurate separation of the excitation torque and its speed response (signal) on the one hand, and the motor control loop executing the RtR movement (noise) on the other hand. As a main contribution, based on the superposition principle for linear systems, this work proposes a method that separates signal and noise, thus reducing the RtR motion time. Moreover, a maximum inertia variation (MIV) and position deviation quality check are developed since system nonlinearities bound the newly proposed estimation technique.

The remainder of this work is structured as follows: chapter 2 briefly explains the estimation principle of [24]. Next, chapter 3 decomposes the cause of failure of the current estimation principle and presents a renewed estimation methodology. Chapter 4 introduces a nonlinearity quality check. Chapter 5 validates the proposed approach using measurements. Finally, chapter 6 concludes the outcome of this work and proposes some future work.

2 Estimation principle

2.1 Machine model

The physical behavior of many industrial single-axis driven machines can eventually be approximated by the two-mass model presented in Fig. 2. The motor's rotor inertia J_r and the driven load inertia J_l are linked via a coupling with stiffness k and damping b properties. As a result, subject to the machine's motion principle, e.g., a rod mechanism inspired pick-and-place unit, the motor often experiences an inertia J_l and load torque T_l that varies as a function of the machine's position θ_l (see Fig. 8) and, therefore, the time t . Friction coefficients represent friction in both the motor b_r and the load b_l . Next, the relation between the motor torque T_m , the load position θ_l , and its derivatives, as described in [23] and derived in Appendix A, is formulated as:

$$\begin{cases} T_m - C_l - b_r \dot{\theta}_r = J_r \ddot{\theta}_r \\ T_l(\theta_l) + C_l - b_l \dot{\theta}_l = \frac{1}{2} \frac{d(J_l(\theta_l))}{d(\theta_l)} \dot{\theta}_l^2 + J_l(\theta_l) \ddot{\theta}_l, \end{cases} \quad (1)$$

with

$$C_l = b(\dot{\theta}_r - \dot{\theta}_l) + k(\theta_r - \theta_l),$$

where θ_r and θ_l represent the motor and load position, respectively. Moreover, equation (1) can be linearised and transformed into the Laplace domain [23], so that the relationship between the input motor torque T_m and the load position θ_l can easily be studied in the frequency domain:

$$\frac{\dot{\theta}_r(s)}{T_m(s)} = \frac{J_l s^2 + (b + b_l)s + k}{J_r J_l s^3 + (J_r(b + b_l) + J_l(b + b_r))s^2 + \dots} \quad (2)$$

$$\dots (k(J_r + J_l) + b_r b_l + (b_r + b_l)b)s + \dots$$

$$\dots (b_r + b_l)k$$

Moreover, preliminary research [24] has shown that especially the frequency region around the resonance and anti-resonance is the most interesting because of the sensitivity of the load inertia J_l and the limited influence of friction b_r and b_l . Therefore, it is reasonable to neglect both the motor and load friction since their impact near this frequency region is neglectable, simplifying the complex model from (2) to:

$$\frac{\dot{\theta}_r(s)}{T_m(s)} = \frac{J_l s^2 + bs + k}{J_r J_l s^3 + (J_r + J_l)bs^2 + (J_r + J_l)ks}. \quad (3)$$

In the remainder of this work, equation (3), describing the system's behaviour near the anti-resonance peak, serves as the basic equation for estimating the position-dependent inertia $J_l(\theta)$.

2.2 Estimation principle

The foundation of this work's estimation principle lies in the determination of a frequency-specific gain between the motor torque T_m on the one hand and the resulting motor speed $\dot{\theta}_r$ on the other hand. Starting from equation (3)'s left term, a gain $G_{f_{est}}$ can be formulated as:

$$G_{f_{est}} = \frac{|\dot{\theta}_r|_{f_{est}}}{|T_m|_{f_{est}}}. \quad (4)$$

Furthermore, the frequency-specific gain $G_{f_{est}}$ can also be determined using the magnitude of equation (3) and the substitution of $s = j\omega_{est}$:

$$G_{f_{est}} = \sqrt{\frac{b^2 \omega_{est}^2 + (J_l \omega_{est}^2 - k)^2}{(J_r J_l \omega_{est}^3 - k \omega_{est} (J_l + J_r))^2 + (b \omega_{est}^2 (J_l + J_r))^2}}. \quad (5)$$

Then, equation (5) can be reformulated as equation (6) in which the load inertia J_l is isolated:

$$J_l = \frac{A \pm \sqrt{B}}{C}$$

with

$$\begin{aligned} A &= (k - b^2)G_{f_{est}}^2 J_r \omega_{est}^3 - (G_{f_{est}}^2 J_r k^2 + 1)k\omega_{est} \\ B &= G_{f_{est}}^2 k^4 + 2G_{f_{est}}^2 b^2 k^2 \omega_{est}^2 + 2G_{f_{est}}^2 J_r^2 b^2 \omega_{est}^6 \\ &\quad + (G_{f_{est}}^2 b^2 - 1)b^2 \omega_{est}^4 - G_{f_{est}}^4 J_r^4 b^2 \omega_{est}^8 \\ C &= G_{f_{est}}^2 J_r^2 \omega_{est}^5 - (2G_{f_{est}}^2 J_r k - G_{f_{est}}^2 b^2 + 1)\omega_{est}^3 \\ &\quad + G_{f_{est}}^2 k^2 \omega_{est}. \end{aligned} \quad (6)$$

Equation (6) allows estimating the load inertia $J_l(\theta_r)$, provided that the other system properties, such as coupling stiffness k and damping b are well known. Thus, the inertia estimation is reduced to estimating the amplitude of both velocity $|\dot{\theta}_r|_{f_{est}}$ and torque $|T_m|_{f_{est}}$ signals at a frequency f_{est} for which the frequency response of the considered model closely approximates reality. The Sliding DFT (SDFT) filter, further deepened in section 2.3., is suggested to estimate these amplitudes.

Furthermore, for high-dynamic industrial positioning applications, it is common to use a classic cascade-controlled PMSM motor. To provide sufficient excitation at the desired frequency f_{est} and allow analysis, [24] proposes to inject an additional sinusoidal torque signal on top of the controller's outgoing torque signal. The resulting combined control and estimation scheme, consisting of a classical cascade controller, excitation torque signal T_{add} , spectral filters, and the actual estimator, is shown in Fig. 3. Moreover, in [25], a guideline on the disturbance-to-position ratio (DPR) was proposed to guarantee the success of the estimate. The DPR is calculated following:

$$DPR = \frac{|T_{add}| \cdot \left| \frac{\dot{\theta}_r(s)}{T_{add}(s)} \right|_{f_{est}}}{\frac{\Delta\theta_{RtR}}{2} \cdot \left| \frac{\dot{\theta}_r(s)}{\theta_r^*(s)} \right|_{f_{RtR}}}, \quad (7)$$

with $|T_{add}|$ the amplitude of the excitation signal, $\left| \frac{\dot{\theta}_r(s)}{T_{add}(s)} \right|_{f_{est}}$ the gain of the machine speed $\dot{\theta}_r$ to the excitation torque T_{add} at the excitation frequency f_{est} , $\Delta\theta_{RtR}$ the RtR trajectory distance to be travelled and $\left| \frac{\dot{\theta}_r(s)}{\theta_r^*(s)} \right|_{f_{RtR}}$ the gain from the desired position to the velocity at f_{RtR} . The frequency f_{RtR} can, in turn, be determined by approximating the RtR position trajectory as a sinusoid with $f_{RtR} = \frac{1}{2t_{RtR}}$, given that t_{RtR} is the time in which the RtR motion is completed. The DPR was experimentally determined to be greater than 0.05 in simulation to ensure the estimation quality.

Note that the gains from equation (7) are mainly determined by the cascade control loop parameters, which for high-dynamic applications usually have to be set optimally so that both gains $\left(\left| \frac{\dot{\theta}_r(s)}{T_{add}(s)} \right|_{f_{est}} \right)$ and $\left(\left| \frac{\dot{\theta}_r(s)}{\theta_r^*(s)} \right|_{f_{RtR}} \right)$ can be considered nonadjustable. Moreover, during the machine design phase, a machine builder typically imposes requirements on both the trajectory and the motion execution time-frame t_{RtR} . And finally, since the system response gain $G_{f_{est}}$ with respect to the load inertia J_l is most sensitive near the anti-resonance region, which led to the reduced model equation (3) in 2.1, the excitation frequency f_{est} is also more or less fixed [24]. Consequently, only the amplitude of the excitation signal $|T_{add}|$ is adjustable and, according to [25], should be chosen large enough so that the prescribed minimum ratio is reached, naturally within the margin of the maximum available motor torque T_{max} .

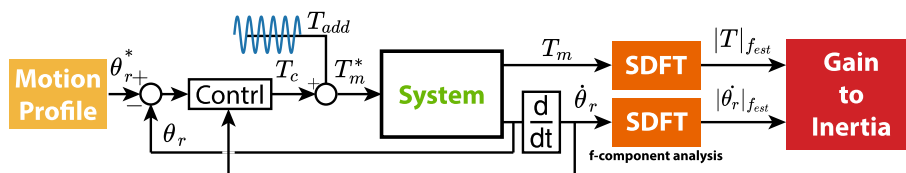


Fig. 3 Conceptual presentation of the inertia estimation principle presented in [24]

2.3 Spectral filter

At base, as explained in section 2.2, the inertia estimator relies on the amplitude estimations of both the motor torque $|T_m|$ and the motor velocity $|\dot{\theta}_r|$ at the chosen excitation frequency f_{est} . The recursive sliding version of the discrete Fourier transform (SDFT) is proposed to estimate both amplitudes computationally efficiently and guarantee online implementation. The SDFT per iteration transfers a full window of equally sampled data from the non-frequency domain (usually the time domain) to the frequency domain following

$$X^k(n) = \left[X^k(n-1) - x(n-N) + x(n) \right] e^{j2\pi \frac{kn}{N}}, \quad (8)$$

with $X^k(n)$ the complex result of the k^{th} harmonic after transformation of the n^{th} recursive sample, $X^k(n-1)$ the complex result of the previous sample, $x(n)$ the newest sample within the considered window and $x(n-N)$ the oldest sample within the considered window. Employing

$$x^k(n) = \frac{1}{N} \sum_{k=0}^{N-1} X^k(n) e^{j2\pi \frac{kn}{N}}, \quad (9)$$

the spectral filtered signal can be reconstructed in the original (time) domain. Next, to analyze the behaviour of the SDFT filter, the combination of the (S)DFT and iDFT (9) is often considered in the complex domain [7]:

$$G_{SDFT}^k(z) = \frac{Z \left[x^k(n) \right]}{Z \left[x(n) \right]} = \frac{1}{N} \frac{1 - z^{-N}}{1 - e^{j2\pi \frac{k}{N}} z^{-1}}. \quad (10)$$

filtering out a one-sided specific harmonic k . Reconstructing the original time signal can be done simply by adding both sides ($+k$ & $-k$) together. Moreover, from (10), it is deduced that the foundation of the SDFT filter consists of a comb-filter $1 - z^{-N}$, a complex resonator $(1 - e^{j2\pi \frac{k}{N}} z^{-1})^{-1}$ and a magnitude/phase correction term $\frac{1}{N}$. While the comb filter introduces N equally spaced zeros on the unit circle in the complex z -plane, the complex resonator introduces a single pole on that same unit circle. Then, by colocating the resonator's pole with one of the zeros, a so-called pole-zero cancellation is obtained, filtering out one specific frequency. Finally, the magnitude/phase correction term rescales the complex result to the signal's original scale. Figure (4) shows the magnitude frequency response of the filter with a fundamental frequency ($k = 1$) of 50Hz and 100Hz, respectively, which are the estimation frequencies for the machine considered in the remainder. Note that due to the lobe structure of the filter, only the fundamental harmonic and its integer multiples are neutralized, and intermediate noise is not completely suppressed.

Finally, starting from the analysis of (8) and (10), one can deduce that the comb-filter introduces a buffer of N samples by removing the oldest sample $n - N$ each time a new sample n is added, thus introducing a delay in the estimation. Therefore, a discrete change in the magnitude of the harmonic content on sample n is only fully corrected N samples later. Accordingly, strongly depending on the dynamics of the signal to be estimated, an SDFT filter introduces, on average, a delay of $\frac{N}{2}$ samples on the filtered magnitude estimate. To correctly estimate the load inertia in either the time or the angular domain, the delay introduced by the SDFT-filter must be compensated, as demonstrated in [24]. For a time-domain inertia estimation, assuming a sampling strategy with a constant time base, the filter's result is best shifted back in time over half a signal period ($\frac{N}{2}$ samples) to minimize the mean error.

3 Spectral filter influences on a dynamic estimation

As explained in chapter 2 and as visually apparent in Fig. 5d, the estimator fails in general at lower motion times due to the under-reached DPR-ratio. As shown in 3.1, the leading cause of failure of the inertia estimator can be boiled down to a mismatch between the spectral content of the torque and velocity signals on the one hand and the characteristics of the SDFT filter on the other hand. Therefore, in sections 3.2 and 3.3, a new method is presented dealing with the DPR-ratio.

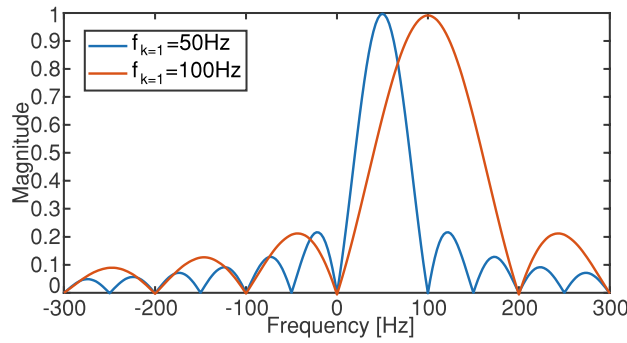


Fig. 4 SDFT-filter magnitude frequency response with fundamental filter frequency of 50Hz (blue) and 100Hz (orange) and harmonic passage at $k = 1$

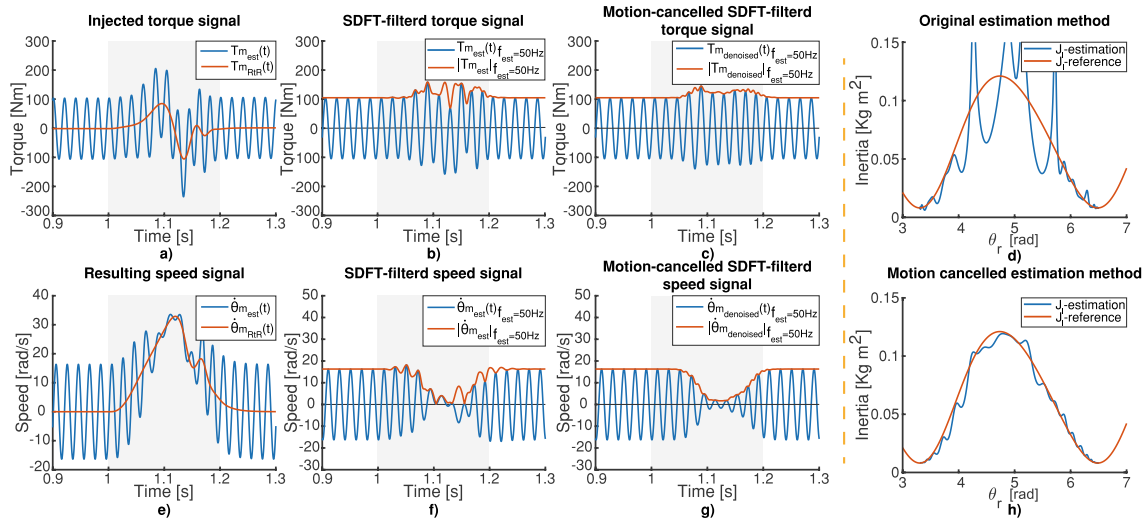


Fig. 5 Demonstration in simulation of the influence of the newly proposed denoising methodology on the position-dependent inertia estimation for an RtR trajectory. ($t_{RTR}^* = 200 \text{ ms}$, $K_{pp} = 60 \frac{\text{rad}}{\text{s}}$, $K_{ps} = 7 \frac{\text{Nm}}{\text{rad}}$, $T_{is} = 8 \text{ ms}$, $T_{add} = 50\%$ of T_{max})

3.1 Failure mechanism

The total ingoing machine torque T_m consists of the motor controller torque T_c and the excitation torque T_{add} . The controller primarily facilitates the execution of the RtR motion, while the excitation torque T_{add} ensures sufficient harmonic content at the desired frequency. The excitation signal has a fixed frequency f_{est} and amplitude $|T_{add}|$ over time. Conversely, due to the rest-to-rest motion, the motor controller torque signal's dominant spectral content varies over time. At both machine rest points, e.g., only the static load torque T_l has to be overcome ($\dot{\theta} = 0$). A torque of varying magnitude is required to realise the desired motion. Thus, the dominant content in the frequency space varies as a function of the required RtR motion time for a generic system. As motion time decreases, the torque magnitude and the maximum spectral frequency will increase. Figure 6a shows the spectrogram of the injected torque signal T_m for a classic 5th-order polynomial RtR trajectory executed at 200 ms. Notice the quasi-stable 50 Hz excitation signal with constant magnitude and the varying RtR torque between 1 s and 1.2 s. For a 2-mass system, in analogy with the torque signal, the resulting velocity frequency spectrum is similar.

Additionally, the estimator relies on the system's excitation torque T_m and speed response $\dot{\theta}_r$ amplitude estimation employing an SDFT filter. So, both signals' excitation frequency spectral content must be separated from the rest of the frequency spectrum caused by the amplitude and frequency variable RtR control and considered by the estimator as 'noise'. As shown in Fig. 4, the SDFT filter's magnitude consists of a lobe structure with unit amplification and amplification roll-off from the pass frequency f_{est} . So, due to the filter's principle, only the DC component and all integer multiples of the pass frequency f_{est} are fully neutralised, while intermediate spectral content is only partially

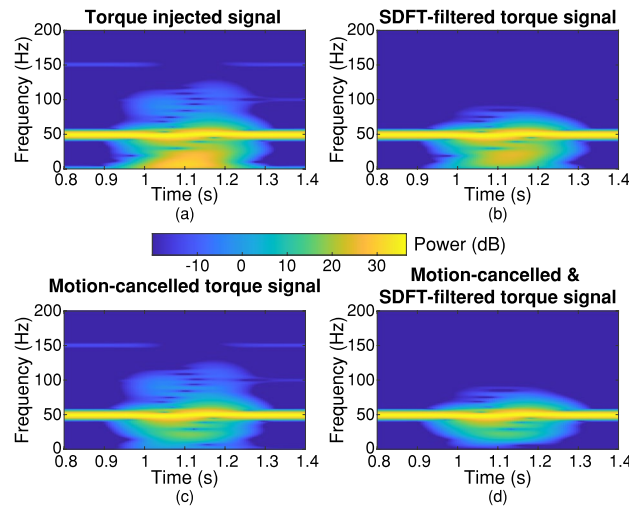


Fig. 6 Spectrogram of a typical a) ingoing system torque T_{mr} , b) SDFT filtered ingoing torque, c) motion cancelled ingoing torque and d) motion cancelled + SDFT filtered torque

suppressed. These non-fully suppressed frequency components are carried through the filter, as shown in Fig. 6b, yet resulting in an erroneous estimate of the harmonic. Eventually, this results in an incorrect inertia J_l estimation. Thus, the leading cause of the estimator's failure can be simplified as the insufficient accurate/dynamic separation of signal and noise due to leakage.

Moreover, in addition to the spectral leakage, the ratio of the 'ground wave' (in our case, the excitation signal) to the RtR noise also plays a vital role in the magnitude of leakage and, thus, failure. As shown in Fig. 4, the SDFT filter rescales its complex result to a unity gain at the pass frequency f_{est} . Consequently, as the signal-to-noise ratio decreases due to, e.g. limited excitation torque or a short motion time, the influence of noise on the magnitude estimate increases. Finally, due to the filter's lobe structure (Fig. 4), noise at frequencies closer to the pass frequency is suppressed worse. Therefore, at faster motion times, due to the higher required motor torque introducing fundamentally higher frequencies, RtR-introduced noise is suppressed less, thus increasing the chance of an erroneous estimate.

In summary, the performance of the current estimation mechanism is thus limited by the spectral filter and the ratio between the excitation signals and RtR controller signals and fails more easily at higher speeds due to spectral noise. [25] previously anticipated this by defining the DPR-ratio from section 2.2 high-enough.

3.2 Enhanced spectral filtering of the torque and speed's magnitude

Fundamentally improving the estimation principle, as shown in the previous section, can be narrowed to enhancing the instantaneous magnitude estimation of both the f_{est} components of input torque T_m and speed $\dot{\theta}_r$ under 'noisy' conditions. Therefore, this work proposes to suppress the 'noise' by subtracting both clean RtR motion torque $T_{m_{RtR}}(t)$ and velocity $\dot{\theta}_{r_{RtR}}(t)$ profiles from respectively time-aligned RtR motion profiles $\dot{\theta}_{r_{est}}(t)$, $T_{m_{est}}(t)$ during estimation:

$$\begin{aligned}\dot{\theta}_{r_{denoised}}(t) &= \dot{\theta}_{r_{est}}(t) - \dot{\theta}_{r_{RtR}}(t) \\ T_{m_{denoised}}(t) &= T_{m_{est}}(t) - T_{m_{RtR}}(t),\end{aligned}\quad (11)$$

resulting in the newly proposed methodology of Fig. 7.

In this work, the considered 2-mass model from Fig. 2 exhibits non-linear behaviour due, among other parameters, the position-dependent inertia $J_l(\theta_l)$ and the load torque $T_l(\theta_l)$. However, superposition can be applied assuming that the machine can be approximated locally linear. To derive equation 11, the linear model from equation (3) is adopted, and further represented by operator S . Also, the system is assumed closed-loop controlled, as in Fig. 7. Hence, the torque $T_{c_{RtR}}(t)$ requested by the motor controller results in a pure RtR motion profile $\dot{\theta}_{r_{RtR}}(t)$:

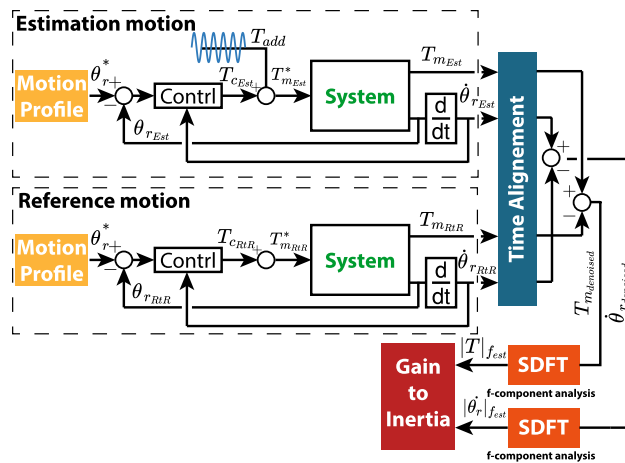


Fig. 7 Newly proposed estimation principle employing a RtR motion cancellation to suppress estimator’s noise

$$S\{T_{m_{RR}}(t)\} = S\{T_{c_{RR}}(t)\} = \dot{\theta}_{r_{RR}}(t) \tag{12}$$

Alternatively, during estimation, the total machine-injected motor torque $T_{m_{est}}(t)$, composed of the additional excitation torque $T_{add}(t)$ and the controller torque $T_{c_{est}}(t)$ executing the RtR movement, ultimately results in the speed $\dot{\theta}_{r_{est}}(t)$. In turn, the controller torque $T_{c_{est}}(t)$ can be subdivided into a part purely responsible for the RtR trajectory $T_{c_{RR}}(t)$ and a fraction that aims to counteract the additional excitation $T_{c_{add}}(t)$ (which the controller considers as noise):

$$\begin{aligned} S\{T_{m_{est}}(t)\} &= \dot{\theta}_{r_{est}}(t) \\ S\{T_{c_{est}}(t) + T_{add}(t)\} &= \dot{\theta}_{r_{est}}(t) \\ \leftrightarrow S\{T_{c_{RR}}(t) + T_{c_{add}}(t) + T_{add}(t)\} &= \dot{\theta}_{r_{est}}(t) \end{aligned} \tag{13}$$

Both preceding scenarios are easily implementable on an industrial drive. Subsequently, by subtracting the torque of the excited $T_{m_{est}}$ and non-excited $T_{m_{RR}}$ motions following the superposition principle, the torque purely responsible for RtR motion $T_{m_{RR}}(t)$ is neutralised. So as a system’s input, the sum of the excitation torque $T_{add}(t)$ and controller counteracting torque $T_{c_{add}}(t)$ remains, resulting in the speed $\dot{\theta}_{r_{denoised}}(t)$

$$\begin{aligned} S\{T_{m_{est}}(t)\} - S\{T_{m_{RR}}(t)\} &= \dot{\theta}_{r_{est}}(t) - \dot{\theta}_{r_{RR}}(t) \\ \leftrightarrow S\{T_{add}(t) + T_{c_{add}}(t)\} &= \dot{\theta}_{r_{est}}(t) - \dot{\theta}_{r_{RR}}(t) \\ \leftrightarrow S\{T_{m_{denoised}}(t)\} &= \dot{\theta}_{r_{denoised}}(t). \end{aligned} \tag{14}$$

Since the additional excitation torque frequency $f_{T_{add}}$ is imposed, and a linear system and speed controller are assumed, both the system speed response $\dot{\theta}_{r_{denoised}}(t)$ and the counteracting response torque $T_{c_{add}}(t)$ will have the same fixed frequency. Besides, the magnitude of the speed, and hence, the magnitude of the counteracting excitation torque and the total machine torque, correlate with the system properties among the load side inertia. Thus, by obtaining $\dot{\theta}_{r_{denoised}}(t)$ and $T_{m_{denoised}}(t)$ over time, the inertia can be estimated ‘noise’-free following the method from chapter 2. Yet, the instantaneous amplitudes $|\dot{\theta}_{r_{denoised}}(t)|$ and $|T_{m_{denoised}}(t)|$ still need to be estimated using, e.g., an SDFT filter. Alternatively to the sliding DFT, the configurable and, therefore, faster converging generalised DFT ($m = 4, l = \pm 1$) was evaluated in simulation [8]. Unfortunately, the profit made by a more dynamic estimation is undermined by a poorer suppression of residual noise. Therefore, the SDFT filter is retained in this work. Again, reconsidering the load torque signal from section 3.1, the result of both the motion denoising and the denoising + SDFT filter are shown in Figs. 6.c and 6.d. Note the apparent improvement in lower harmonic content between the original (Fig. 6a) and the newly proposed method.

Table 1 Properties of the considered machine model in simulation

Motor			Coupling		Load
T_{max} [Nm]	J_r [kgm ²]	br [Nms/rad]	k [Nm/rad]	b [Nms/rad]	bl [Nms/rad]
233	0.012	0.2	24963	8.62	0.1

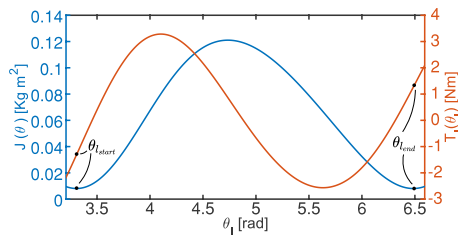


Fig. 8 Position-dependant inertia $J(\theta_i)$ and load torque $T_l(\theta_i)$ of both the considered simulation model (3.3) and the physical machine

3.3 Simulation results

To evaluate the effectiveness of the proposed method, in simulation, the inertia $J(\theta_i)$ of the system described by the parameters summarized in Table 1 and Fig. 8, is estimated during an RtR motion of 200 ms given an additional torque injection with an amplitude $|T_{add}|$ of 50% of maximum torque T_{max} at $f_{est} = 50$ Hz. The excited and non-excited torque and velocity profiles are respectively shown in Fig. 5a and e. Next, given these signals, subplots 6b and 6f show the SDFT filtered signals with corresponding amplitude following the original method (without noise reduction). Subplots 6c and 6g show the SDFT filtered signals according to the newly proposed method after first applying the proposed denoising. Note that, e.g., the amplitude of the filtered velocity signal under the original method contains more substantial fluctuations than the new method.

Finally, subplots 6d and 6h, respectively, show the inertia estimation following the original and new methods. As visually apparent, the original method fails, while the proposed denoising of both signals yields a good estimate. The remaining imperfections can be attributed to the dynamics of the SDFT filter and the influence of the non-linearity of the considered machine (see chapter 3).

4 Limitations of the renewed estimation method

Section 3 revealed the estimator’s cause of the failure at faster motion times and showed that clever filtering increases the estimator’s deployability. However, as visible in Fig. 9, the estimator fails when further reducing the motion time using an estimation frequency f_{est} of 50 Hz. The denoising principle proposed in section 3.2 assumes that the considered

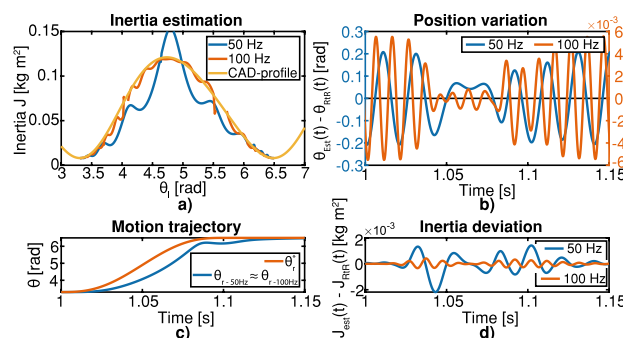


Fig. 9 Effect of the excitation frequency f_{est} on the non-linear behaviour of the model and accompanying estimation accuracy. ($t_{RTR}^* = 100$ ms, $K_{pp} = 60 \frac{rad}{s}$, $K_{ps} = 7 \frac{Nms}{rad}$, $T_{is} = 8$ ms, $T_{add} = 20\%$ of T_{max})

nonlinear model exhibits approximate linear behaviour, allowing the superposition principle to suppress the estimator's noise. The failure of the estimator is suspected to be caused by excessive variation in inertia J_l within a single excitation period $1/f_{est}$, resulting in a more pronounced response from the controller and consequently distorting the torque and velocity at the estimation frequency. Therefore, in the case of quasi-constant load inertia, employing the new method no longer limits the minimal motion time at all. The previous estimator [25] does set boundaries to the maximal estimation speed, even under the assumption of constant inertia over time. Nevertheless, the applicability area of the newly proposed estimator is again limited by non-neglectable variations in the inertia, introducing nonlinearities undermining the denoising principle. Consequently, a method is required to restrict the estimator's applicability.

4.1 Cause and restraints for non-linear machine behaviour

For the considered model, non-linear behaviour is caused by the position-dependent load torque $T_l(\theta_l)$ and inertia $J_l(\theta_l)$. Since the nonlinearities are primarily due to inertia, the load torque is further neglected. In terms of inertia J , the impact of the position dependency strongly correlates with the inertia gradient $\frac{dJ}{dt}$ over time and the excitation signal-induced position error $\theta_{Est} - \theta_{RtR}$. The smaller the inertia gradient $\frac{dJ}{dt}$ over time, the smaller the excitation signal's impact. Moreover, given the sinusoidal nature of the excitation signal, the average excitation signal's contribution to the machine position is zero. Thus, the smaller the signal's magnitude $|T_{add}|$, and the higher its excitation frequency f_{est} , the lower the induced position error and, thus, the better the nonlinearities. Also, the position controller helps to reduce the position error since its main task is to execute the pre-described RtR trajectory.

In summary, the estimator's range can be maximised by a) choosing the highest possible estimation frequency f_{est} combined with the lowest allowable amplitude of the torque signal $|T_{add}|$. A higher frequency f_{est} results in a minor local position variation and thus inertia variation, as shown in Figs. 9b and d (note the difference between the left and right axis). And b) by minimising the inertia variation over time $\frac{dJ}{dt}$. The latter can be done by choosing motion profiles where the maximum rotor speed $\dot{\theta}_r$ is lower, such as e.g. a standard 1/3 motion profile. Figure 9 shows the estimator's result for an RtR movement of roughly $t_{RtR} = 100 \text{ ms}$ at both f_{est} 50 Hz and 100 Hz to demonstrate the effect of the estimation frequency on the system nonlinearities. As apparent in subplot a), the estimation fails for a 50 Hz signal, while the 100 Hz estimation nicely follows the theoretical CAD-extracted inertia profile.

4.2 An estimation quality check

Since the estimation may fail, a validation method is necessary to verify the estimation quality. After all, if the inertia profile is unknown, simulation shows that a deviation due to excessive nonlinearities cannot be easily derived visually from the course of the estimated inertia profile itself. In addition, it is challenging to establish a conclusive analytical formulation to evaluate the accuracy. To statistically validate the extent to which two signals are linearly related over time, e.g. the denoised torque and speed signals, the magnitude-squared coherence (MSC) is often used in the literature [12]. However, the MSC requires a multiple of the fundamental signal period (at least two, but often more) to yield a meaningful result. Given the dynamics of the estimation, in practice, only a limited number of estimation periods per motion cycle exist so that the coherence is an averaged value over the entire estimation period. Unfortunately, simulations showed that the average coherence is not the right measure to evaluate the estimation quality.

Simulations, however, show that a combination of the estimated inertia variation (IV) and the denoised position signal $\theta_{r,denoised}$ are good guides to the estimation reliability. In simulation, through trial-and-error, an excessively fast variation of the inertia profile per excitation period can be arbitrarily linked to an erroneous estimate. Therefore, in this work, the maximum inertia variation MIV is defined as:

$$MIV = \max(|IV(i)|) = \max(|J_i - J_{i-N}|) \quad (15)$$

with $J(i)$ the i 'th inertia estimation sample and N the total number of samples per excitation period. As a guideline, given various observations, for both considered estimation frequencies, all estimates with an instantaneous MIV below 0.05 were successful. Estimates with MIV between 0.05 and 0.08 are typically more choppy and sometimes unreliable. Estimates with peak values above 0.08 were always unreliable. Illustrative Figs. 10a–c show the estimation result $J_l(\theta_r)$, instantaneous inertia variation IV and estimation error $\epsilon J_l(\theta_r)$ for different motion times and frequencies, respectively. Moreover, in addition to the MIV , bright deviant behaviour is also well reflected in the denoised position signal:

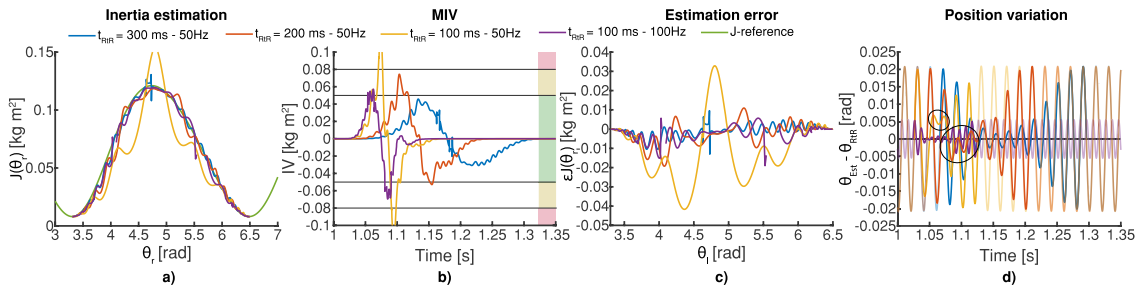


Fig. 10 Demonstration of the influence of the newly proposed denoising methodology on the position-dependant inertia estimation for an RtR trajectory. ($t_{RTR}^* = 200\text{ ms}$, $K_{pp} = 60 \frac{\text{rad}}{\text{s}}$, $K_{ps} = 7 \frac{\text{Nms}}{\text{rad}}$, $T_{is} = 8\text{ ms}$, $T_{add} = 50\%$ of T_{max})

$$\theta_{r_{denoised}}(t) = \theta_{r_{est}}(t) - \theta_{r_{RtR}}(t) \tag{16}$$

with $\theta_{r_{est}}(t)$ the actual position trajectory travelled during an estimate, and $\theta_{r_{RtR}}(t)$ the actual position trajectory of the reference motion. Ideally, the perfectly ingoing sinusoidal torque results in a sinusoidal denoised position trajectory with varying amplitude due to the variable inertia, as shown in Fig. 10d in blue and purple. As experimentally observed, a too-strong deviation from a perfect sinusoid indicates a too-rapid inertia variation, resulting in an erroneous estimate. As circled in Fig. 10d, if the MIV is high, a DC component arises locally in the denoised position signal $\theta_{r_{est}}$. The size of this DC component can be seen as a measure of nonlinearity. However, as with the estimation, the calculated MIV is subject to correct values for the stiffness k and damping b . Therefore, a combined check with the MIV and the denoised position signal is recommended to check for nonlinearities.

5 Validation

The methodology proposed in Sects. 3 and 4 is validated using the mechanism presented in Fig. 11. For validation, the machine’s position-dependent inertia is estimated at different motion times using a standard 1/3 motion profile and two different injection frequencies.

5.1 Validation mechanism and motion platform

The motor’s datasheet inertia was used as the validation application’s driving inertia J_r . As load inertia $J_l(\theta_r)$, is the inertia to be estimated, a CAD model was used to extract the inertia as a function of the motor position θ_r for validation purposes [21]. The load inertia J_l and the load torque T_l are visualised in Fig. 8. Moreover, Fig. 12 shows the corresponding machine’s system response as a function of frequency. As deduced from the system response, the machine’s dynamic behaviour can be simplified to the two-mass model presented in Fig. 2. Employing the response, the stiffness k and damping b values of the machine’s coupling were determined and further tuned using the reference estimation result from section 5.2. The theoretical system response following the model described by equation (3) is also shown in Fig. 12. The theoretical and measured responses are mainly similar. Finally, by analogy with the procedure in [24], possible estimation frequencies f_{est} of 50 and 100 Hz were derived.

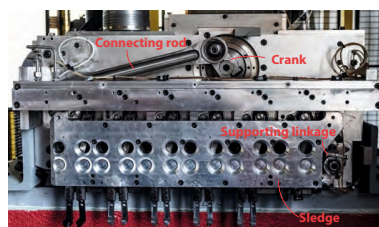


Fig. 11 The application used to validate the newly established estimation method

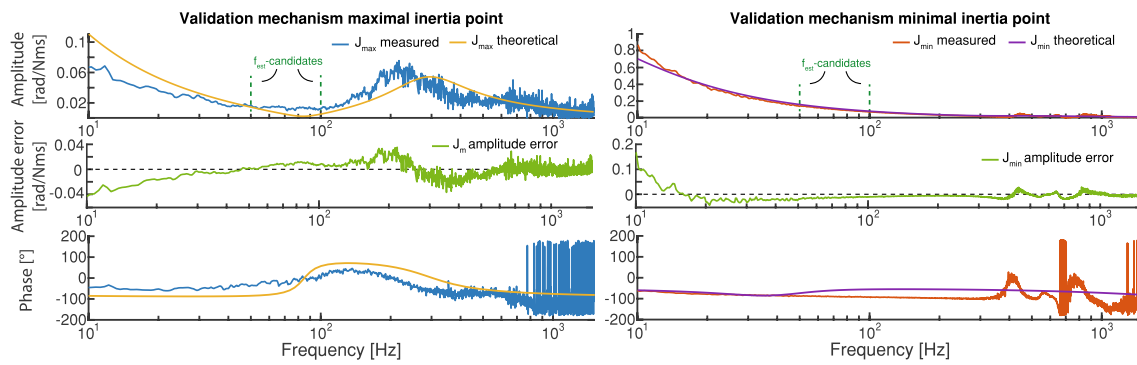


Fig. 12 Measured bodes of the validation mechanism at both minimal and maximal inertia positions. Moreover, surplus to the measured bodes, for both positions, the theoretical two-mass system bodes, tuned employing the measured bodes, are visualized. One can see that the bode characteristic changes due to a change in load inertia. Finally, the amplitude errors between the measured and tuned bodes are given

All measurements were performed via Beckhoff’s commercial motion platform, Twincat Engineering. Therefore, the method worked out is relatively easily implementable and, thus, quickly deployable.

5.2 Reference estimation

As a baseline for the minimum required motion time t_{RtR} , the considered machine’s inertia $J_l(\theta_r)$ is estimated using the previously published method [24, 25]. For the selected controller settings Kpp , Kps , Tn , injected torque amplitude $|T_{add}|$ and estimation frequency f_{est} of 50Hz, a DPR ratio of 0.075 was achieved at a desired motion time t_{RtR}^* of 500ms. A generic 1/3 profile is used as the desired position setpoint θ_r^* signal. The controller values were tuned to limit the maximum tracking error to a few degrees. Any form of feedforward was disabled. Figure 13 shows the estimation result with associated error $\epsilon J(\theta_r)$ as a function of machine position θ_r . Similarly, the position trajectory $\theta_r(t)$, speed $\dot{\theta}_r(t)$ and torque signal during the estimation $T_m(t)$ are shown over time. Since, as a reference, the old method is regarded, in the light of chapter 3.2, solely the estimation signals $\dot{\theta}_{r_{est}}(t)$ and $T_{m_{est}}(t)$ are used. A statistical analysis

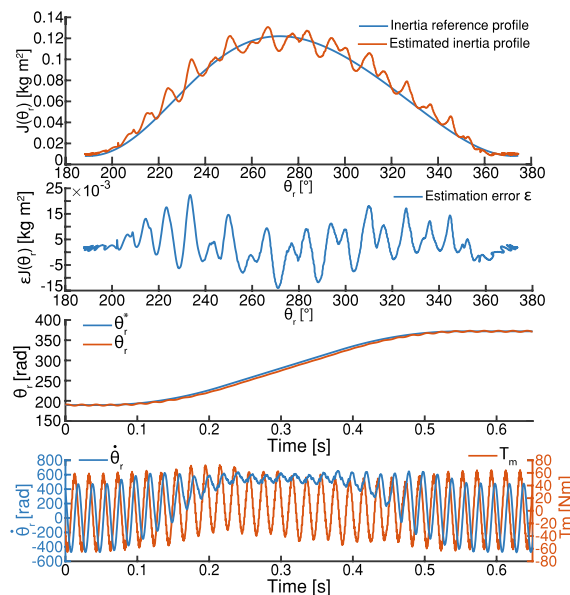


Fig. 13 Inertia reference estimation according to the former published method explained in chapter 2, without denoised torque and velocity signals ($t_{RtR}^* = 500\text{ ms}$, $f_{est} = 50\text{ Hz}$, $Kpp = 100 \frac{\text{rad}}{\text{s}}$, $Kps = 5.65 \frac{\text{Nms}}{\text{rad}}$, $Tn = 8\text{ ms}$, $T_{add} = 20\%$ of T_{max} , $DPR = 0.075$)

Table 2 Statistical analysis of the estimation results with respect to the CAD-extracted inertia profile

Case	t_{RtR}^* [ms]	RMSE [kgm ²]	σ [kgm ²]	$\epsilon J(\theta_r)_{max}$
Reference	500	0.0073	0.0066	0.0224
New method	300	0.0068	0.0054	0.0160
	250	0.0059	0.0058	0.0150
	200	0.0070	0.0069	0.0185

of the estimation result with respect to the CAD-extracted inertia profile is summarised in table 2. Note that the estimation result is already quite inaccurate, so the motion time was not pushed further from a DPR of 0.075 to 0.05.

Similarly, estimates were performed at 100 Hz. However, in line with previous publications, this estimation frequency results in a non-significant result, making it unusable for further analysis ($T_{sample} = 125\text{ ms}$).

5.3 Validation measurements

Three estimate attempts with a motion time t_{RtR}^* of 0.3 s, 0.25 s and 0.2 s, respectively, were performed to validate the newly proposed method. A 1/3 profile was used as the desired position trajectory θ_r^* . The position trajectory θ_r and accompanying estimation variables were measured for each considered motion time during movements with and without additional torque T_{add} . Subsequently, the speed $\dot{\theta}_r(t)$ and torque $T_m(t)$ signals were denoised for each motion time t_{RtR}^* , followed by the actual inertial estimate $J_l(\theta_r)$. The speed and torque signals can easily be aligned using the drive's start command trigger. Finally, both the MIV and position variation $\theta_{Est} - \theta_{RtR}$ are calculated.

For each motion time $t_{RtR}^*(t)$, the estimation result $J_l(\theta_r)$, the error on the estimate $\epsilon J_l(\theta_r)$, the MIV, position variation $\theta_{Est} - \theta_{RtR}$, the position trajectory $t_{RtR}(t)$ and the denoised velocity $\dot{\theta}_{r,denoised}(t)$ and torque signals are displayed in Fig. 14. Again, the statistical analysis of the estimation result is summarised in table 2.

Given the values of the root-mean-squared error RMSE on the estimation result $J_l(\theta_r)$, the standard deviation σ of the estimation error $\epsilon J_l(\theta_r)$, and the maximum estimation error value $\epsilon J_l(\theta_r)_{max}$, one can observe that the motions with an RtR time of 0.3 s en 0.25 s score better than the reference trajectory of 0.5 s from section 5.2 using the old [24] estimation method. Moreover, note that the MIV, shown in Fig. 14b, ascends above 0.05 at a motion time of 0.2 s. Thus, according to the guideline in section 4.2, this estimate is considered less reliable. Besides, in the position variation shown in Fig. 14d, apparent local deviations can be observed, circled in black, reinforcing the MIV exceedance. To conclude, using the newly elaborated method on this machine, the desired RtR time t_{RtR}^* can be halved while estimating without quality deterioration in comparison with the earlier published estimator [24, 25].

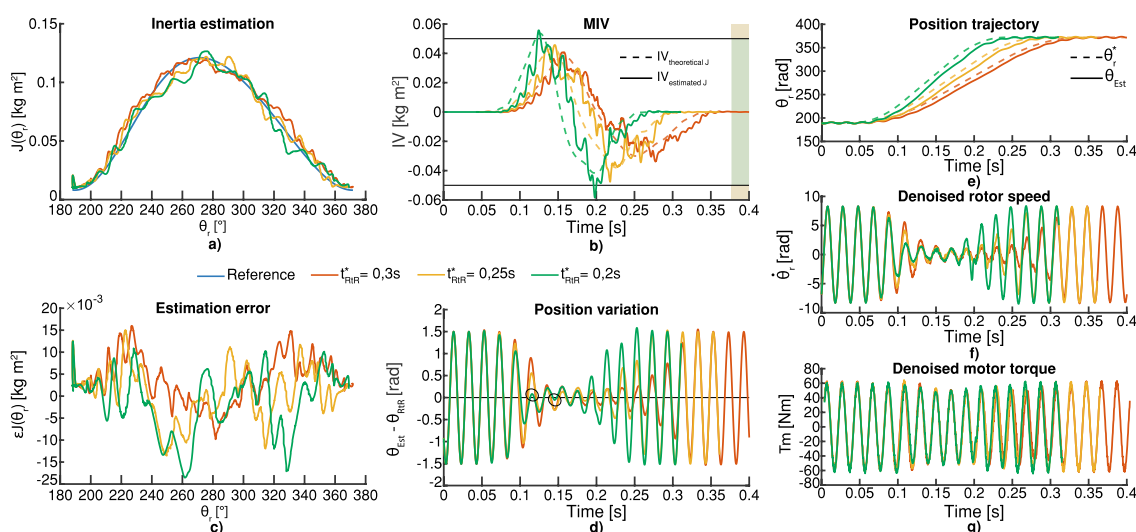


Fig. 14 Estimation of the load-side inertia of the machine in Fig. 11 at three different motion times following the execution of a trapezoidal RtR position trajectory ($f_{est} = 50\text{ Hz}$, $K_{pp} = 100 \frac{\text{rad}}{\text{s}}$, $K_{ps} = 5.65 \frac{\text{Nm s}}{\text{rad}}$, $T_n = 8\text{ ms}$, $T_{add} = 20\% \text{ of } T_{max}$)

6 Conclusion

By elaborating on an earlier published method [24, 25], this paper aims to lower the minimum achievable motion time, allowing a position-dependent inertia estimation. In the long run, this information enhances the machine's real-time performance, i.e. by using this for motion profile optimisation as in [25]. This work revealed that the present estimator's failure mechanism at fast motion times is due to the insufficient separation of the spectral content at the estimation frequency and other spectral energy introduced by the rest-to-rest motion. Therefore, as its main contribution, this work presents the idea of stripping the velocity and torque estimation signal of spectral noise prior to estimation by subtracting the non-exited from the exited speed and torque signals so that the latter is disposed of by spectral noise caused by the rest-to-rest motion. Consequently, the newly developed estimation principle is no longer bounded by the motion time or related speed but rather by the (non-)linear behaviour of the considered machine. Given the maximum allowed nonlinearities, to assess/guarantee the quality and accuracy of the inertia estimation, this work proposes a maximum inertia variation (MIV) metric, which should be lower than 0.05.

To demonstrate the impact of the proposed methodology, on a physical machine, three estimation attempts with a motion time of 0.3 s, 0.25 s and 0.2 s, respectively, were performed. Utilising the original methodology [24], a baseline motion time of 0.5 s was found as a reference. By employing the new methodology, the minimum achievable motion time was halved to 0.25 s without exceeding the predetermined quality control criteria and without statistically sacrificing the quality of the estimation itself. Future work can focus on analyzing the cause of failure at higher estimation frequencies (different positions in the bode plot), as this would lower machines' nonlinearities' impact on the estimate and thus shorten the required motion time. Alternatively, given prior inertia information, evaluating if the proposed method is applicable to estimate the machine's damping can be interesting.

Author contributions All authors contributed to the study of Online tracking of dynamically time-varying inertia using an enhanced SDF-based estimation methodology. David Ceulemans, Foeke Vanbecelaer, and Stijn Derammelaere performed the initial conceptualization. David Ceulemans, Nick Van Oosterwyck, and Stijn Derammelaere performed the data collection and analysis. David Ceulemans wrote the first draft of the manuscript, and all authors commented on previous versions of the manuscript. All authors read and approved the final manuscript.

Funding An internal PhD grant from the University of Antwerp funded this research.

Data availability The data presented in this study are available upon request from the corresponding author.

Code availability No code is available.

Declarations

Competing interests The authors declare no competing interests.

Open Access This article is licensed under a Creative Commons Attribution 4.0 International License, which permits use, sharing, adaptation, distribution and reproduction in any medium or format, as long as you give appropriate credit to the original author(s) and the source, provide a link to the Creative Commons licence, and indicate if changes were made. The images or other third party material in this article are included in the article's Creative Commons licence, unless indicated otherwise in a credit line to the material. If material is not included in the article's Creative Commons licence and your intended use is not permitted by statutory regulation or exceeds the permitted use, you will need to obtain permission directly from the copyright holder. To view a copy of this licence, visit <http://creativecommons.org/licenses/by/4.0/>.

Appendix A Derivation of the torque equations for a two-mass position-varying-inertia system

Consider a two-mass system (see Fig. 2) with a fixed rotor inertia J_r and load inertia J_l varying as a function of the system's position θ_l . Moreover, the system is subject to a driving motor torque T_m and load torque T_l , which depends on the system position θ_l . In addition, both system masses are subject to frictional torques $T_{friction}$, which can be described using the friction coefficients b_r, b_l and the system speeds $\dot{\theta}_r, \dot{\theta}_l$. Since friction drains energy from the system, the system is non-conservative. Finally, the connection between both masses is described by a spring k and damper b component in parallel. For this two-mass model, in general, the kinetic energy K , the potential energy V , and the compensating term Q used in the Euler-Lagrange equation for non-conservative systems can be described as:

$$\begin{aligned}
K &= \frac{1}{2} J_r \dot{\theta}_r^2 + \frac{1}{2} J_l(\theta_l) \dot{\theta}_l^2 \\
V &= \frac{1}{2} k(\theta_r - \theta_l)^2 \\
Q_{\theta_r} &= T_{motor} - b \cdot (\dot{\theta}_r - \dot{\theta}_l) - b_r \dot{\theta}_r \\
Q_{\theta_l} &= T_{load}(\theta_l) + b \cdot (\dot{\theta}_r - \dot{\theta}_l) - b_l \dot{\theta}_l
\end{aligned} \tag{A1}$$

Then, the Lagrangian L is defined as:

$$L = K - V = \frac{1}{2} J_r \dot{\theta}_r^2 + \frac{1}{2} J_l(\theta_l) \dot{\theta}_l^2 - \frac{1}{2} k(\theta_r - \theta_l)^2 \tag{A2}$$

So that:

$$\frac{d}{dt} \left(\frac{\partial L}{\partial \dot{\theta}} \right) - \frac{\partial L}{\partial \theta} = Q_\theta \tag{A3}$$

The partial derivative of L to θ_r , θ_l , $\dot{\theta}_r$ and $\dot{\theta}_l$ results in

$$\begin{aligned}
\frac{\partial L}{\partial \theta_r} &= -k(\theta_r - \theta_l), \\
\frac{\partial L}{\partial \theta_l} &= \frac{1}{2} \dot{\theta}_l^2 \left(\frac{\partial J(\theta_l)}{\partial \theta_l} \right) + k(\theta_r - \theta_l), \\
\frac{\partial L}{\partial \dot{\theta}_r} &= J_r \dot{\theta}_r, \\
\frac{\partial L}{\partial \dot{\theta}_l} &= J_l(\theta_l) \dot{\theta}_l.
\end{aligned} \tag{A4}$$

So that

$$\begin{aligned}
\frac{d}{dt} \left(\frac{\partial L}{\partial \dot{\theta}_r} \right) &= J_r \ddot{\theta}_r, \\
\frac{d}{dt} \left(\frac{\partial L}{\partial \dot{\theta}_l} \right) &= \frac{d(J(\theta_l))}{dt} \frac{d\theta_l}{dt} \dot{\theta}_l + J(\theta_l) \ddot{\theta}_l = \frac{d(J(\theta_l))}{d\theta_l} \dot{\theta}_l^2 + J(\theta_l) \ddot{\theta}_l.
\end{aligned} \tag{A5}$$

Therefore, finally, the equilibrium equations for each individual mass system can be derived:

$$\begin{aligned}
\frac{d}{dt} \left(\frac{\partial L}{\partial \dot{\theta}_r} \right) - \frac{\partial L}{\partial \theta_r} &= Q_{\theta_r} \\
\leftrightarrow T_{motor} - b_r \dot{\theta}_r &= J_r \ddot{\theta}_r + k(\theta_r - \theta_l) + b \cdot (\dot{\theta}_r - \dot{\theta}_l)
\end{aligned} \tag{A6}$$

$$\begin{aligned}
\frac{d}{dt} \left(\frac{\partial L}{\partial \dot{\theta}_l} \right) - \frac{\partial L}{\partial \theta_l} &= Q_{\theta_l} \\
\leftrightarrow T_{load}(\theta_l) - b_l \dot{\theta}_l &= J_l(\theta_l) \ddot{\theta}_l \\
+ \frac{1}{2} \frac{d(J(\theta))}{d\theta} \dot{\theta}_l^2 - k(\theta_r - \theta_l) - b \cdot (\dot{\theta}_r - \dot{\theta}_l)
\end{aligned} \tag{A7}$$

References

1. Bermudez JCM, Bershada NJ. Transient and tracking performance analysis of the quantized lms algorithm for time-varying system identification. *IEEE Trans Signal Process.* 1996;44(8):1990–7.
2. Ceulemans D, Van Oosterwyck N, De Viaene J, et al (2022) Time-optimal bang-bang driven rest-to-rest motion through an angular switching point. 2022 IEEE/ASME International Conference on Advanced Intelligent Mechatronics (AIM) pp 1639–1645. <https://doi.org/10.1109/aim52237.2022.9863247>
3. Chen JS, Huang CL. Dynamic analysis of flexible slider-crank mechanisms with non-linear finite element method. *J Sound Vib.* 2001;246(3):389–402. <https://doi.org/10.1006/jsvi.2001.3673>.
4. Chen T, He H, Chen G, et al. Parameter identification for nonlinear time-varying dynamic system based on the assumption of “short time linearly varying” and global constraint optimization. *Mech Syst Signal Process.* 2020;139: 106620. <https://doi.org/10.1016/j.ymssp.2020.106620>.
5. De Mathelin M, Lozano R. Robust adaptive identification of slowly time-varying parameters with bounded disturbances. *Automatica.* 1999;35:1291–305. <https://doi.org/10.23919/ECC.1997.7082448>.
6. Li Y, Wei H, Billings SA. Identification of time-varying systems using multi-wavelet basis functions. *IEEE Trans Control Syst Technol.* 2011;19(3):656–63. <https://doi.org/10.1109/TCST.2010.2052257>.
7. Liu H, Hu H, Chen H, et al. Fast and flexible selective harmonic extraction methods based on the generalized discrete fourier transform. *IEEE Trans Power Electron.* 2018;33(4):3484–96. <https://doi.org/10.1109/TPEL.2017.2703138>.
8. Liu H, Hu H, Chen H, et al. Fast and flexible selective harmonic extraction methods based on the generalized discrete fourier transform. *IEEE Trans Power Electron.* 2018;33(4):3484–96. <https://doi.org/10.1109/TPEL.2017.2703138>.
9. Liu K, Wang R, Zheng S, et al. Fixed-time disturbance observer-based robust fault-tolerant tracking control for uncertain quadrotor uav subject to input delay. *Nonlinear Dyn.* 2022;107(3):2363–90. <https://doi.org/10.1007/s11071-021-07080-0>.
10. Liu Z, Xu J, Fang H. Extracting Inherent Model Structures and Identifying Parameters of Time-Varying Systems Using Local Linear Neuro-Fuzzy Networks. *IEEE Trans Fuzzy Syst.* 2022;30(1):233–47. <https://doi.org/10.1109/TFUZZ.2020.3034972>.
11. Malik S, Enzner G. Fourier expansion of Hammerstein models for nonlinear acoustic system identification. *ICASSP, IEEE Int Conf Acoustics Speech Signal Process Proceed.* 2011;1:85–8. <https://doi.org/10.1109/ICASSP.2011.5946334>.
12. McCarthy DJ. Short-time coherence functions: instantaneous and tuned. *Mech Syst Signal Process.* 1997;11(2):169–85. <https://doi.org/10.1006/mssp.1996.0073>.
13. Na J, JuanYang, Ren X, et al (2014) Robust adaptive estimation of nonlinear system with time-varying parameters. *International Journal of Adaptive Control and Signal Processing (February):*1055–1072. <https://doi.org/10.1002/acs.2524>
14. Na J, Xing Y, Costa-Castello R. Adaptive estimation of time-varying parameters with application to Roto-Magnet plant. *IEEE Trans Syst Man Cybernet Syst.* 2021;51(2):731–41. <https://doi.org/10.1109/TSMC.2018.2882844>.
15. Nevaranta N, Derammelaere S, Parkkinen J, et al. Online identification of a two-mass system in frequency domain using a Kalman filter. *Model Identification Control.* 2016;37(2):133–47. <https://doi.org/10.4173/mic.2016.2.5>.
16. Nevaranta N, Derammelaere S, Parkkinen J, et al. Online identification of a mechanical system in frequency domain using sliding DFT. *IEEE Trans Indus Electron.* 2016;63(9):5712–23. <https://doi.org/10.1109/TIE.2016.2574303>.
17. Pai S, Neuberger B, Buchholz M (2021) Online estimation of mass and moment of inertia of cargo bike payload using an unscented kalman filter. 21 st International Conference on Control, Automation and Systems pp 806–811. <https://doi.org/10.23919/ICCASS2745.2021.9649971>
18. Perdomo M, Pacas M, Eutebach T, et al. Identification of variable mechanical parameters using extended Kalman Filters. *Proceedings - 2013 9th IEEE International Symposium on Diagnostics for Electric Machines. Power Electron Drives SDEMPED.* 2013;2013:377–83. <https://doi.org/10.1109/DEMPED.2013.6645743>.
19. Schuette F, Beineke S, Rolfsmeier A, et al. Online identification of mechanical parameters using Extended Kalman Filters. *Conf Record IAS Anni Meeting IEEE Industry Appl Soc.* 1997;1(2):501–8. <https://doi.org/10.1109/ias.1997.643069>.
20. Van Der Merwe R, Wan EA (2004) Sigma-point kalman filters for probabilistic inference in dynamic state-space models. PhD thesis
21. Van Oosterwyck N, Vanbecelaere F, Haemers M, et al (2019) Cad enabled trajectory optimization and accurate motion control for repetitive tasks. *IEEE 15th International Conference on Control and Automation* <https://doi.org/10.1109/ICCA.2019.8899728>
22. Van Oosterwyck N, Yahya AB, Cuyt A, et al (2020) CAD based trajectory optimization of PTP motions using chebyshev polynomials. *IEEE/ASME International Conference on Advanced Intelligent Mechatronics, AIM 2020-July:*403–408. <https://doi.org/10.1109/AIM43001.2020.9158893>
23. Vanbecelaere F, Derammelaere S, Knockaert J, et al (2020a) Identification of dynamic systems with position dependent load parameters. *7th International Conference on Control, Mechatronics and Automation (ICCMA)* pp 38–43. <https://doi.org/10.1109/ICCMA46720.2019.8988773>
24. Vanbecelaere F, Derammelaere S, Nevaranta N, et al (2020b) Online tracking of varying inertia using a sdft approach. *Mechatronics* 68(July 2019). <https://doi.org/10.1016/j.mechatronics.2020.102361>
25. Vanbecelaere F, Van Oosterwyck N, Derammelaere S, et al. On-line motion profile optimization for reciprocating mechanisms. *Mech Mach Theor.* 2022;173(March): 104833. <https://doi.org/10.1016/j.mechmachtheory.2022.104833>.